J. Membrane Biol. 94, 267–278 (1986)

The Journal of
Membrane Biology

Serial Permeability Barriers to Water Transport in Human Placental Vesicles

Nicholas P. Illsley and A.S. Verkman
Division of Nephrology, Cardiovascular Research Institute, University of California, San Francisco, California 94143

Summary. Microvillous vesicles were prepared from term human placenta by shearing, differential centrifugation and Mg^{2+} precipitation. Vesicles were purified further on a sucrose density gradient producing two bands with densities of 1.16 to 1.18 g/ml (C1) and 1.13 to 1.15 g/ml (C2). The C2 fraction, which had a 24-fold enrichment of alkaline phosphatase and a three-fold reduction in Na^+, K^+-ATPase activity compared to homogenates, was used to measure osmotic water (P_f) permeability. P_f was measured from the time course of scattered light intensity following exposure of vesicles to specified gradients of impermeant solutes. P_f decreased from 3.0×10^{-3} to 0.6×10^{-3} cm/sec with increasing gradient size (65 to 730 mM; 23°C). Four possible causes of this behavior were examined theoretically and experimentally: an unstirred layer, saturation of water transport, large changes in the vesicle surface area with changes in volume and a structural restriction to vesicle volume change. The measured dependence of P_f on gradient size and the effect of the channel-forming ionophore gramicidin on P_f fit best to the theoretical dependences predicted by a structural restriction mechanism. This finding was supported by experiments involving the effects on P_f of increased solution viscosity, initial vesicle volume, the magnitude of transmembrane volume flow, and the effects of gradient size on activation energy (E_a) for P_f. The decreased P_f resulting from a structural restriction limiting vesicle volume change was modeled mathematically as a second barrier in series with the vesicle membrane. E_a measured using a 250-mM inwardly directed sucrose gradient was 5.4 ± 0.6 kcal/mol ($T >$ 27°C) and 10.0 ± 0.6 kcal/mol ($T <$ 27°C). E_a above 27°C is in the range normally associated with transmembrane passage of water via aqueous channels. Water transport was not inhibited by *p*-chloromercuribenzenesulfonate.

Key Words human placenta · water transport · microvillous membrane vesicles · light scattering · urea transport

Introduction

One of the most important features of placental transfer is the exchange of water between mother and fetus. The rate of exchange across the human placenta has been estimated as approximately 60 ml/min in both maternofetal and fetomaternal directions [16]; however, the pathways for water transport and the permeabilities of individual cell membranes have not been defined. Two general mechanisms have been proposed for transcellular water transport. The solubility-diffusion mechanism postulates that water partitions into the lipid membrane and diffuses across between areas of free volume created by thermal fluctuations of the lipid hydrocarbon chains [3, 28]. The other path is via water-filled channels, either formed as transient pores in the lipid membrane or through "fixed" protein-mediated sites [15]. Neither the mechanism of transcellular water transport nor its possible contribution to total transplacental water flow have been characterized.

A vesicle preparation derived from the apical brush border (microvillous membrane) of the human placenta was used to examine placental membrane water permeability. Permeability coefficients and activation energies for microvillous vesicle water transport were determined using stopped-flow light-scattering techniques. These techniques have been used previously to study transport in plasma membrane vesicles isolated from the kidney [35], intestinal mucosa [39], stomach [27] and brain [36].

This report describes a decrease in the osmotic permeability coefficient with increasing gradient size resulting from a structural restriction. This structural limitation, which was modeled mathematically as a second barrier in series with the vesicle membrane, has not been reported previously in either vesicles or cells. Placental brush-border water transport is also unique among vesicle systems in showing a low activation energy at higher temperatures (>27°C) and a higher activation energy below 27°C. The activation energy above 27°C is comparable to that associated with transmembrane passage of water through aqueous channels.

Materials and Methods

Vesicle Preparation

The preparation of microvillous vesicles was a modification of methods described by Bissonnette et al. [2], Booth et al. [4] and Truman et al. [33]. Term human placental tissue (38 to 41 weeks gestational age) was obtained within 20 min of delivery and placed on ice. All subsequent steps were carried out at 4°C. The umbilical cord, amniotic and chorionic membranes and the chorionic plate were removed, the tissue was cut into ~1 cm fragments and placed in 0.9% NaCl. After washing twice in 0.9% NaCl and twice in 1.5% $CaCl_2$, the tissue was minced in a meat grinder. 250 g of tissue were stirred in 2 volumes of buffer A (250 mM sucrose, 10 mM HEPES-Tris, pH 7.0) at low speed (<60 rpm) for 60 min, filtered through gauze and the filtrate centrifuged at 2500 × *g* for 10 min. Solid $MgCl_2$ was added to the supernatant to a concentration of 12 mM and the mixture was stirred slowly for 60 min and centrifuged at 2,500 × *g* to remove the Mg^{2+}-precipitated, nonmicrovillous membranes. The resulting supernatant was centrifuged at 48,000 × *g* for 30 min to sediment the vesicles. The pellet was resuspended in 150 ml of buffer A containing 20 mM NaCl and centrifuged at 48,000 × *g* for 60 min to produce a crude microvillous vesicle pellet (fraction C).

Placental homogenates (fraction H), used for determining vesicle purification, were prepared by homogenizing minced tissue in 4 volumes of buffer A in a Sorvall Omni-Mix at full speed for 4 min. The homogenate was then filtered through gauze to remove any gross particulate matter (<5%) and stored at −70°C.

Vesicles were purified further by sucrose density gradient centrifugation. Initially fraction C (~75 mg protein) was suspended in 9 ml of buffer A and 3-ml portions were layered on to a 28 to 42% (wt/vol) sucrose gradient containing 10 mM HEPES-Tris, pH 7.0. The gradient was centrifuged for 16 h in a Beckman SW 28.1 rotor at 28,000 rpm (144,000 × *g*). Gradients were collected in 2-ml fractions, sucrose concentrations determined by refractometry and fractions were assayed for marker enzyme activities. In later preparations, fraction C was resuspended in 45 ml of buffer A and 15-ml aliquots were layered on 20 ml of 35% (wt/vol) sucrose containing 10 mM HEPES-Tris, pH 7.0, and centrifuged in the SW 28.1 rotor for 60 min at 144,000 × *g*. The interfacial layer was collected and diluted to 150 ml with buffer A and centrifuged at 48,000 × *g* for 30 min to produce the final vesicle pellet (fraction C2). This fraction and that which sedimented to the bottom of the sucrose gradient (fraction C1) were resuspended in buffer A and frozen at −70°C.

Biochemical and Morphological Characterization of Vesicles

Alkaline phosphatase, aminopeptidase M, acid phosphatase, Na^+, K^+-ATPase, NADPH-cytochrome *c* reductase and succinate dehydrogenate were assayed by published methods [6, 13, 19, 29, 34]. Gamma-glutamyl transferase was assayed using a reagent kit (Sigma Chemical Company, St. Louis, Mo.). All enzyme assays were carried out at 23°C. Protein concentration was measured by the method of Lowry et al. [23] in the presence of 0.2% deoxycholate. Protease activity in vesicle preparations was assayed by measuring the release of acid-soluble dye from azocasein after incubation with vesicles for 4 hr at 37°C. Osmolarities were measured using an Advanced Wide-Range Osmometer model 3W2.

SDS-polyacrylamide gel electrophoresis was carried out by the method of Laemmli [22], using reagents obtained from Bio-Rad (Richmond, Calif.). Vesicle samples were heated to 95°C for 4 min in the SDS sample buffer. Samples (25 to 50 μg protein) were loaded onto 1.5-mm slab gels (4.0% stacking gel; 10.0% separating gel) which had been pre-electrophoresed at 20 mA/slab for 60 min. The gels were run at 25 mA/slab through the stacking gel and 35 mA/slab through the separating gel. Gels were stained with 0.2% Coomassie Blue R-250 in 40% methanol, 10% acetic acid for 2 hr and destained through several changes of 40% methanol, 10% acetic acid. Molecular weights were determined using the standards carbonic anhydrase (29,000 daltons), ovalbumin (45,000), bovine serum albumin (66,000), phosphorylaes b (97,000) and beta-galactosidase (116,000). Laser densitometry was carried out using an LKB UltroScan XL densitometer.

Microvillous membranes were pelleted in 1% Agarose in buffer A and fixed in a modified Karnovsky's fixative [21] for 2 hr. Samples were then rinsed with 0.1 M cacodylate buffer, pH 7.4, and post-fixed in reduced OsO_4 [10] for 1 hr at room temperature. The tissue was then rinsed, dehydrated and embedded in a Poly-bed:Araldite mixture. Sections were examined using a JEOL JEM 100B microscope.

Stopped-Flow Measurements

Stopped-flow measurements were performed on a Dionex-130 stopped-flow apparatus (Sunnyvale, Calif.) which has a dead time of 2 msec and is temperature controlled between 5 and 60°C. 0.1 ml of solution containing vesicles (~0.3 mg protein/ml) was mixed with an equal volume of hypo- or hyperosmotic solutions. The time course at 90° scattered light intensity at 500 nm was recorded by a MINC/23 computer (Digital Equipment, Maynard, Mass.) for subsequent analysis. No change in light scattering was observed when vesicles were mixed with isosmotic solutions. Where used, gramicidin was added from ethanol stock (25 mg/ml) to give a final concentration of 10 μg/ml membrane protein. Addition of an equivalent volume of ethanol to vesicles did not affect the rate of water transport.

P_f was calculated from the time course of scattered light intensity by comparing single exponential time constants fitted to the data with single exponential time constants fitted to simulated curves in which P_f was varied. Simulated curves were calculated from the equations,

$$dV(t)/dt = P_f(S/V_o)\bar{v}_w[C_i(t=0)/V(t) - C_o] \quad (1)$$

$$I(t) = a + b[V(t)] + c[V(t)]^2 \quad (2)$$

where $V(t)$ is vesicle volume normalized to volume at $t = 0$, S/V_o is initial vesicle surface-to-volume ratio, $\bar{v}_w$ is the partial molar volume of water, $C_i\,(t = 0)$ is initial intravesicular osmolarity, C_o is solution osmolarity, $I(t)$ is scattered light intensity and a, b and c are constants determined experimentally (*see below*) which relate scattered light intensity to vesicle volume. Equations (1) and (2) are solved iteratively using the initial volume, $V(0)$, appropriate for the experiment.

Results

Sucrose Gradient Separations

Centrifugation of fraction C on a continuous sucrose density gradient (28 to 42% wt/vol) produced

Table 1. Alkaline phosphatase and Na^+, K^+-ATPase activities in placental homogenates and microvillous vesicle fractions C, C1 and C2[a]

Fraction	Alkaline phosphatase	Na^+, K^+-ATPase	Relative[b] enrichment
Homogenate	130 ± 28	12.0 ± 1.0	1
C	2802 ± 810	13.0 ± 0.2	20
C1	1550 ± 551	6.2 ± 0.5	23
C2	3230 ± 1036	3.1 ± 0.8	96

[a] Enzyme activities (nmol/min/mg membrane protein) are mean ± SD for four placental preparations.
[b] The values for relative enrichment were obtained by dividing the alkaline phosphatase/Na^+, K^+-ATPase ratio for all fractions by the same ratio for the homogenate.

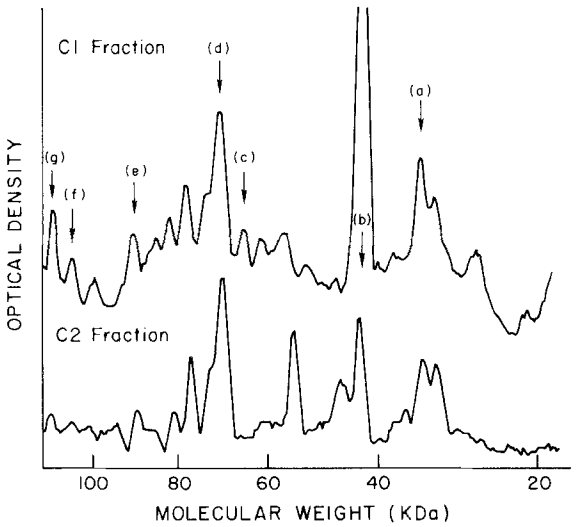

Fig. 1. Densitometric tracings of SDS/polyacrylamide gels of protein in MVV fractions C1 and C2. 50 μg of membrane protein solubilized from C1 and C2 was electrophoresed in 10% gels and stained with Coomassie Blue R-250. Densitometry traces show the intensity of the stained gel bands plotted against molecular weight (daltons) for a typical set of C1 and C2 fractions. The molecular weight scale was constructed using a quadratic function calculated from the positions of the molecular weight markers. Bands which showed a reproducible difference in five separate placental preparations are marked with arrows: (*a*) 37,000, (*b*) 42,000 (*c*) 64,000 (*d*) 71,000 (*e*) 93,000 (*f*) 104,000 (*g*) 115,000

two peaks of alkaline phosphatase activity at densities of 1.16 to 1.18 g/ml (fraction C1) and 1.13 to 1.15 g/ml (fraction C2). We used the nomenclature of Truman et al. [33] to describe the sucrose gradient bands containing the microvillous vesicles. The fractions corresponding to these two bands of activity were collected, resuspended in buffer A and centrifuged separately on 35% (wt/vol) sucrose step gradients. The C2 fraction sedimented to the interface layer while the C1 fraction pelleted below the 35% sucrose layer, confirming the separate identities of the two fractions and the fact that they were not interconvertible. The activities of two plasma membrane markers were assayed in placental homogenates and vesicle fractions C, C1 and C2 (Table 1). Alkaline phosphatase is a marker for the microvillous membrane while ouabain-inhibitable Na^+,K^+-ATPase is a marker for the basolateral membrane of the syncytiotrophoblast. The enrichment of alkaline phosphatase (specific activity/homogenate specific activity) in C2 was 25-fold compared to 12-fold for the C1 fraction. The relative enrichment (alkaline phosphatase/Na^+,K^+-ATPase) compared to basolateral membrane was 96-fold for C2 compared to 23-fold for the C1 fraction.

SDS/Polyacrylamide Gel Electrophoresis

The electrophoretic patterns of fractions C1 and C2 after Coomassie Blue staining of the SDS gels were similar but there were a number of distinct, reproducible differences. Figure 1 shows typical densitometry scans of the C1 and C2 fractions. Each band was quantified as the area under the peak relative to total area. Proteins of approximate molecular weight, 37,000, 44,000, 64,000, 93,000, 104,000 and 115,000 were more abundant (20 to 50%) in C1 than C2, whereas a protein of molecular weight 71,000 was more abundant (30 to 40%) in C2. These findings were observed in vesicle samples from five separate placental preparations. A number of other changes were observed between C1 and C2 in individual preparations which were not reproducible across all five preparations and were not considered relevant in the comparison.

To ensure that the electrophoretic patterns were not modified by endogenous protease activity, samples from the C, C1 and C2 fractions were assayed for protease activity. The protease activity of trypsin was more than 30,000-fold greater (on a per mg protein basis) than any of the microvillous vesicle samples demonstrating the absence of significant protease activity in these fractions (*data not shown*).

We chose to use the C2 vesicle fraction (microvillous vesicles; MVV) in all subsequent investigations because of its greater purity as defined by the higher alkaline phosphatase and lower Na^+, K^+-ATPase activities. Approximately 30 to 45 mg of membrane protein were obtained in the C2 fraction prepared from 250 to 300 g of placental tissue.

Marker Enzyme Assays

Aminopeptidase M was assayed as an additional marker for the microvillous plasma membrane,

Table 2. Marker enzyme activities in homogenate and C2 fraction microvillous vesicles from human placenta[a]

Enzyme	Homogenate	C2 Fraction	Enrichment
Alkaline phosphatase	124 ± 38	2911 ± 536	23.5
Aminopeptidase M	1.7 ± 0.1	3.6 ± 0.3	2.1
Ouabain-sensitive Na^+, K^+-ATPase	5.5 ± 3.2	1.7 ± 0.7	0.3
Succinate dehydrogenase	87 ± 23	6 ± 2	<0.1
NADPH-cytochrome *c* reductase	19.9 ± 3.5	3.4 ± 1.8	0.2
Acid phosphatase	7.8 ± 2.2	1.2 ± 0.8	0.15

[a] Enzyme activities are mean ± SD for four placental preparations in nmol/min/mg membrane protein except for amninopeptidase which is measured in arbitrary fluorescence units/min/mg.

NADPH-cytochrome *c* reductase was assayed for the presence of endoplasmic reticulum, succinate dehydrogenase activity was measured to determine mitochondrial contamination of the MVV and acid phosphatase activity was assayed as a marker for contamination by lysosomal membranes. Table 2 shows the specific activities of these enzymes in the homogenates and MVV from four separate placental preparations.

Electron Microscopy

Electron micrographs of the MVV from four preparations showed a mixed population of microvillous vesicles and microvilli with a higher proportion of the latter. The microvillous dimensions were in the range 0.1 to 0.2 μm diameter and 0.2 to 0.4 μm in length. Few structures (<1%) were observed which were greater in size, showing a lack of contamination by cells, nuclei and mitochondria.

Vesicle Light Scattering

The time course of light scattering when MVV in buffer A (~0.3 mg/ml) were mixed with sucrose buffer to give 250, 375 or 500 mM inwardly directed gradients (1.9, 1.5, and 1.3 Osm^{-1}) is shown in Fig. 2 (top). The time course represents water efflux produced by a hyperosmotic gradient. Also shown is the best-fit single exponential for this data as determined by a least-squares fitting procedure. Similar results were obtained by substituting urea or NaCl for sucrose as the impermeant solute (impermeant on the time scale of water movement). The exponential time constants for water efflux were 0.084 ± 0.006, 0.083 ± 0.005 and 0.083 ± 0.004 sec for 400 mOsm gradients of sucrose, urea and NaCl, respectively (23°C; $n = 6$); thus water flow is independent of the impermeant solute used. No differences were noted between the exponential time constants for water efflux for freshly prepared MVV (0.084 ± 0.006 sec; $n = 6$) and from MVV which had been frozen at −70°C (0.085 ± 0.006 sec; $n = 6$).

Relation Between Scattered Light Intensity and Vesicle Volume

To measure osmotic water permeability coefficients, it was necessary to establish the relationship between the intensity of scattered light and vesicle volumes. There was a linear relationship between entrapped vesicle volume (as measured by [^{3}H]-glucose) and inverse external solution osmolarity in the range 1 to 6 Osm^{-1} (*data not shown*), in agreement with the findings of several investigators [2, 7, 9]. The change in scattered light intensity when MVV in buffer A were mixed with a series of hyperosomotic and hypoosmotic sucrose solutions is shown in Fig. 2 (bottom). The amplitude of the stopped-flow time course was converted to fractional change in scattered light intensity by assigning a value of unity to the light-scattering amplitude of MVV mixed with isosmotic solutions. The decrease in fractional intensity with decreased solution osmolarity (increased Osm^{-1}) was fitted to a quadratic function between 1 and 4 Osm^{-1}. Above 4 Osm^{-1}, the decrease was approximately linear with decreasing osmolarity but small in comparison with that seen below 4 Osm^{-1}. The relationship between vesicle volume and scattered light intensity established by these results was used in subsequent calculations of osmotic permeability coefficients.

Osmotic Water Permeability Coefficient

A series of water efflux and influx curves were generated when MVV in buffer A were mixed with hyper- and hypoosmotic sucrose solutions. The time

constants obtained from the exponential fit to the time course were used to calculate the osmotic water permeability coefficients (P_f) as described in Materials and Methods. The surface-to-volume ratio used was 3.2×10^5 cm^{-1}, calculated assuming microvillous dimensions of 0.15×0.4 μm [20], in agreement with the dimensions observed in the electron micrographs of the MVV. The relationship between P_f and osmotic gradient size ($C_o - C_i$) at 23°C is plotted in Fig. 3.[1] For $C_o - C_i < 65$ mM, P_f was relatively constant at 3.0×10^{-3} cm/sec; for $C_o - C_i > 65$ mM, P_f decreased markedly with increasing gradient size.

There are several possible explanations for the decrease in P_f with increasing gradient size: 1) a solution or intravesicular unstirred layer (USL) forming a flow-dependent serial barrier to transport; 2) saturation of a water transport mechanism such as a specific carrier; 3) large alterations in vesicle surface area with changes in vesicle volume; 4) a structural limitation which restricts the rate of vesicle volume change, equivalent to a second barrier in series with the membrane.

A number of experiments were designed to distinguish among these possibilities. The rationale and results for these experiments are detailed below. Table 3 lists the predicted outcome for each of the mechanisms given above.

Dependence of P_f on Gradient Size

A simple model was developed for each mechanism to generate the predicted dependence of P_f on gradient size. These curves are shown in Fig. 3 plotted with the experimental data. For a USL it is necessary to consider both transient and steady-state USL's. The duration of the USL transient following solution mixing (representing the time required to develop the full solute diffusion polarization gradient) can be estimated from $t_{1/2} = a_v(d^2/D)$ [1], where $t_{1/2}$ is the half-time of the transient (sec), a_v is a dimensionless constant, d is the USL thickness (μm) and D is solute diffusion coefficient in the USL (cm^2/sec). Assuming $d = 0.075$ μm (half the vesicle diameter), $D = 10^{-6}$ cm^2/sec and $a_v = 0.38$ (no volume flow), $t_{1/2} = 20$ μsec, more than three orders of magnitude smaller than the shortest time constant for water efflux. Transient USL phenomena were not therefore included in the calculation of the predicted effects of a USL on P_f. The changes in P_f resulting from a steady-state USL were calculated from the expression for osmotic water flow, modified to include the effect of the USL on the effective external impermeant concentration at the membrane surface during osmotic water flow such that,

$$J_v = P_f^m S\bar{v}_w[C_o\exp(-J_v(d/D)) - C_i]. \quad (3)$$

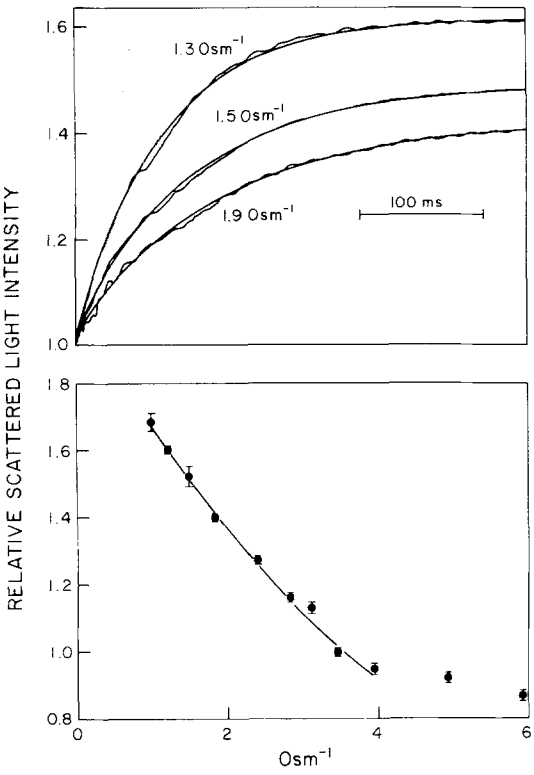

Fig. 2. Scattered light intensity as a function of time and external osmolarity. (Top) Time course of scattered light intensity for microvillous vesicles exposed to a sucrose gradient. Plot of scattered light intensity as a function of time for a suspension of MVV in buffer A after exposure at zero time to 250, 375 or 500 mM inwardly directed sucrose gradients (1.9, 1.5, 1.3 Osm^{-1}). The amplitudes of the stopped-flow time courses were converted to fractional change in scattered light intensity by assigning a value of unity to the scattering amplitude of MVV mixed with isosmotic solutions. Also shown is the best fit single exponential curve for the experimental traces. The exponential time constants were 0.114, 0.092 and 0.068 sec, respectively. (Bottom) Scattered light intensity as a function of Osm^{-1}. MVV diluted in buffer A were mixed with an equal volume of hyper- and hypoosmotic sucrose solutions containing 10 mM HEPES-Tris, pH 7.0. The ordinate represents the amplitude of a single exponential fitted to the time course of scattered light intensity. The data were fitted to the empirical quadratic function $1.02 - 0.38$ [Osm^{-1}] $+ 0.03$ [Osm^{-1}]^2

[1] It is assumed that all vesicle volume is osmotically active. We have examined whether this assumption could modify the calculated decrease in P_f with increasing osmotic gradient size. If f is the fraction of osmotically active vesicle volume, then the $C_i(t = 0)/V(t)$ term in Eq. (1) would be replaced by $fC_i(t = 0)/[V(t) - (1 - f)V(0)]$. In an extreme case where f is taken to be 0.5, calculated P_f would decrease from 6.1×10^{-3} to 2.2×10^{-3} cm/sec as osmotic gradient size increases from 50 to 1000 mOsm.

Table 3. Predicted results of experiments to test proposed mechanisms

Experiments to test proposed mechanisms	1. Unstirred layers	2. Transport saturation	3. Surface area alteration	4. Structural limitation
A. Prediction of the relation between P_f and gradient size	*see* Fig. 3 for predicted curves			
B. Effect of gramicidin on the relation between P_f and gradient size	*see* Fig. 4 for predicted curves			
C. Effect of increased viscosity on P_f	Decrease P_f	No change	No change	No change
D. Effect of pre-shrinking MVV on P_f	No change	No change	Decrease P_f	Decrease P_f[a]
E. Effect of gramicidin on P_f in pre-shrunk MVV	Blunted increase in P_f	Increase P_f	Increase P_f	Blunted increase in P_f
F. Effect of increased gradient size on the activation energy for water transport ($T > T_c$)	Change in E_a to ~5 kcal/mol	Increase in E_a	No change in E_a	Not predictable
G. Effect of increased flow on P_f	Decrease P_f	Decrease P_f	No change	Not predictable[a]

[a] The structural limitation mechanism may be subdivided into two categories: limitation based on the absolute vesicle volume (static structural limitation) or limitation based on the rate of volume change (dynamic structural limitation). Under conditions of the pre-shrink experiment (*D*) given in the text, the former type would show a decrease in P_f whereas the latter type would show no change. Under conditions of the flow dependence experiment (*G*), a dynamic structural restriction would show a decrease in P_f whereas the response with a static structural limitation is not predictable.

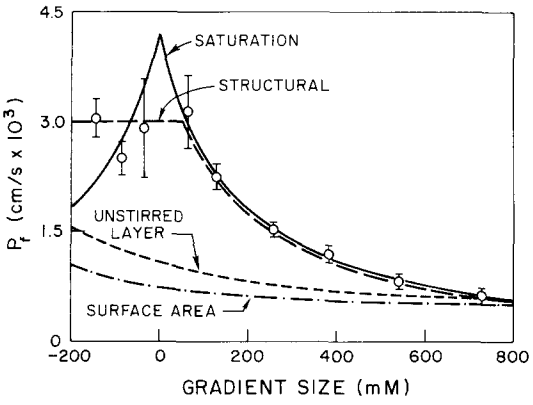

Fig. 3. Dependence of P_f on gradient size. The predicted dependences of P_f on gradient size for a series of models proposed to account for the decrease in P_f with increasing positive gradient are shown by the smooth curves. The theoretical models used to generate these curves are taken from Eqs. (3), (4) and (5) in the text for the USL, transport saturation and structural restriction mechanisms, respectively. The curve for the surface area mechanism was calculated from a modification of Eq. (1) as described in the text. The data points shown by the open circles are the experimental values of P_f calculated from the time course of light scattering after MVV diluted in buffer A were mixed with equal volumes of a series of hypo- and hyperosmotic sucrose solutions (mean ± SD; $n = 8$)

J_v is the water flow (nl/sec), S is the vesicle surface area (cm^2), $\bar{v}_w$ is the molar volume of water (cm^3/mol), P_f^m (cm/sec) is the osmotic water permeability coefficient in the absence of a USL, C_i is the internal impermeant concentration and $C_o\exp(-J_v(d/D))$ is the effective external impermeant concentration (mol/liter). Values for $P_f^m S\bar{v}_w$ and d/D were chosen so that the calculated P_f was equal to the measured value for P_f at the maximum gradient used experimentally (730 mM). The predicted dependence of P_f on gradient size was generated iteratively by solving Eq. [3] for J_v ($= P_f(C_o - C_i)$) for varying C_o. The theoretical curve calculated by this method did not fit the experimental data.

If the decrease in P_f was caused by saturation of a symmetrical transport mechanism, the experimental data should approximately fit a saturable single-site binding model,

$$P_f = P_f^{o'} + \frac{P_f^o\,|[C_o - C_i]|}{|[C_o - C_i]| + K_D} \qquad (4)$$

where P_f^o is the saturable permeability, $P_f^{o'} - P_f^o$ is a nonsaturating permeability and K_D is the osmotic gradient at which the saturable component is half

saturated. The data in Fig. 3 were fitted to Eq. (4) with $P_f^o = 4.4 \times 10^{-3}$ cm/sec, $P_f^{o'} = 4.2 \times 10^{-3}$ cm/sec and $K_D = 165$ mM (Fig. 3). Although the model curve fitted the positive gradient data well, the negative gradient data was not well fitted.

The effect of changes in vesicle surface area (and hence surface-to-volume ratio; S/V) was modeled by altering the calculation of P_f (as described in Materials and Methods) so that S/V_o in Eq. (1) was multiplied by $(V(t)/V(0))^{2/3}$ where $V(t)$ and $V(0)$ are vesicle volumes at time t and time zero. The 2/3 exponent was used to model the isotropic contraction of a sphere or other closed structure. The curve produced by surface area changes (Fig. 3) was plotted such that at maximum gradient the value for P_f from the model was equal to that determined experimentally. The surface area curve did not fit the experimental data. Even if the multiplication factor used was $(V(t)/V(0))^3$, the surface area curve did not fit the experimental data. To fit this data would require a unique type of surface area change such that a small volume decrease produces a very large, nonlinear decrease in surface area.

A structural limitation mechanism was modeled as a second barrier or resistance in series with the membrane resistance ($1/P_f^m$),

$$P_f = (1/P_f^m + R[C_o - C_i])^{-1} \quad (5)$$

where R is a structural resistance factor in units of cm² sec/mol. Equation (5) can be rearranged to give,

$$P_f = P_f^m - \frac{P_f^m R[C_o - C_i]}{1 + R[C_o - C_i]} \quad (6)$$

which is similar to Eq. (4) for a single-site binding model. The dependence of P_f on gradient size is therefore the same as that of the transport saturation curve at higher positive gradients. However, structural restriction is unlikely to be symmetric and it is probable that at some lower gradient it will cease to be an influence on vesicle size. This is shown by the structural limitation curve in Fig. 3 which, at lower gradients remains constant at approximately 3.0×10^{-3} cm/sec.

The Effect of Gramicidin on P_f

In a recent report the channel-forming ionophore gramicidin was shown to increase water permeability in the intestinal brush border [39]. In the placental brush-border membrane P_f increased from $(1.8 \pm 0.1) \times 10^{-3}$ cm/sec to $(3.1 \pm 0.2) \times 10^{-3}$ cm/sec by gramicidin (10 μg/mg membrane protein) at 23°C

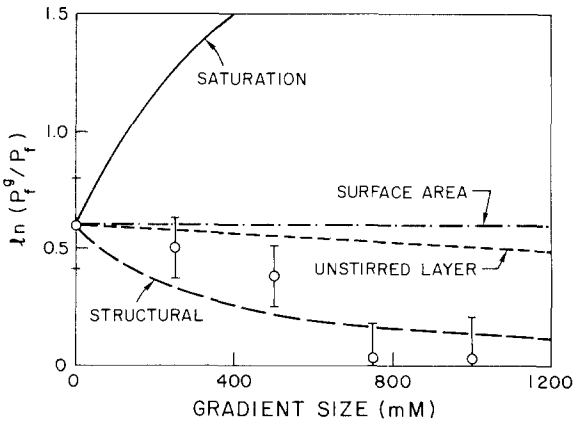

Fig. 4. Effect of gramicidin on P_f. The predicted difference between P_f in the presence and absence of gramicidin (plotted as ln (P_f^g/P_f)) is plotted against gradient size (mM) for the models listed in Table 3. The theoretical curves were calculated using Eqs. (6) and (7) for the transport saturation and structural restriction mechanisms, and using a modification of Eq. (3) for the USL mechanism, as described in the text. The individual points represent differences in P_f values obtained experimentally from the time course of light scattering in the presence and absence of 10 μg gramicidin/mg protein (mean ± SD; $n = 6$)

on exposure to a 250-mM inwardly directed sucrose gradient. The difference between ln (P_f) in the presence ln (P_f^g) and absence of gramicidin ln (P_f) (ln P_f^g/P_f) is plotted against gradient size in Fig. 4 along with the predicted curves for each of the proposed mechanisms causing decreases in P_f with increasing gradient size. The differences in ln (P_f) rather than in P_f were chosen for the plot to separate maximally the predicted effects of gramicidin for each proposed mechanism.

The models described above were modified to include the gramicidin effect. To calculate P_f in the presence of gramicidin for MVV with a steady-state USL, the P_f^m value in Eq. (3) was replaced by an increased value representing $P_f^m + P_f^g$ which, along with the parameters $P_f S\bar{v}_w$ and d/D were adjusted to give the same value of $(P_f^g - P_f^m)$ at zero gradient as the experimental data.

For transport saturation, the gramicidin effect was calculated by including a nonsaturating component for gramicidin (P_f^g) in the single-site binding model as well as the nonsaturating component previously introduced in Eq. (4),

$$P_f = P_f^{o'} - P_f^o \frac{|[C_o - C_i]|}{|[C_o - C_i]| + K_D} + P_f^g \quad (7)$$

where P_f^g was determined experimentally for a small positive gradient. The values of P_f^o, $P_f^{o'}$ and K_D used in this calculation were those determined

previously from the fit of the experimental data to Eq. (4).

For the surface area effect, the fractional increase in P_f caused by gramicidin is independent of osmotic gradient size. Thus P_f^g/P_f (or $\ln P_f/P_f^g$)) is independent of gradient size as shown in Fig. 4. For the structural limitation mechanism, Eq. (5) was modified to give

$$P_f = (1/(P_f^m + P_f^g) + R[C_o - C_i])^{-1} \quad (8)$$

where P_f^g is defined as for Eq. (7). This model gave the closest fit to the experimental data.

Viscosity and Unstirred Layers

When viscosity is increased in a USL (decreased D), increased solute polarization decreases the effective osmotic gradient size resulting in a decreased P_f. In the absence of an unstirred layer, increased viscosity will not affect P_f. The rate of water efflux was measured in the presence and absence of 6% dextran which increased solution viscosity > threefold. The time constant for water efflux for a 500-mM inwardly directed sucrose gradient was 0.082 ± 0.004 sec (n = 8) in the absence of dextran and did not differ significantly from the time constant measured in the presence of dextran (0.077 ± 0.009 sec; n = 8).

Effect of Vesicle Preshrinking on P_f

Comparison of P_f determined using identical initial osmotic gradients (identical volume flow) in normal volume and preshrunken MVV discriminates among several P_f alteration mechanisms as summarized in Table 3. The two flow-dependent mechanisms, USL and transport saturation, would not be affected by a decrease in initial vesicle volume. In the case of the surface area mechanism a decrease in initial vesicle volume will result in a decrease in surface area and a consequent decrease in P_f. Structural restriction becomes increasingly important as vesicle volume is reduced and so preshrinking is predicted to cause a decrease in P_f. This is true for structural limitation based on the absolute volume (static structural limitation) but not for restriction based on the rate of volume change (dynamic structural limitation). Shrinking vesicles prior to measurement of P_f was carried out by suspending MVV in hyperosmotic buffers immediately prior to the stopped-flow experiment. P_f was measured following exposure to identical osmotic gradients for vesicles at isosmotic volume and vesicles shrunken to half the isosmotic volume. P_f determined for isosmotic MVV using a 250-mM sucrose gradient was (1.82 ± 0.12) × 10^{-3} cm/sec whereas that determined for MVV with half the volume was (1.18 ± 0.09) × 10^{-3} cm/sec. The experimental data is in agreement with the predictions for the surface area and static structural restriction models.

A USL or structural restriction mechanism can be viewed as a resistance in series with the primary membrane barrier. Modification of membrane permeability by addition of gramicidin decreases only the membrane resistance. The effects of gramicidin on P_f would therefore be blunted when these mechanisms are operative. In MVV with initial isosmotic volume, gramicidin increased P_f (250 mM inwardly directed gradient) from (1.82 ± 0.12) to (3.06 ± 0.19) × 10^{-3} cm /sec. However, the effect of gramicidin on pre-shrunken MVV P_f was blunted; P_f increased from (1.18 ± 0.09) to (1.93 ± 0.03) × 10^{-3} cm/sec. The blunted gramicidin effect supports the predictions for either a USL or structural restriction mechanism.

Activation Energy for Water Transport

In the presence of a USL, an increased osmotic gradient should increase the fractional resistance due to the USL. The activation energy (E_a) for water transport should therefore tend toward that for solute diffusion in aqueous solution, ~5 kcal/mol. In the presence of a saturating water transport mechanism, increasing the osmotic gradient size should increase the fraction of water transport taking place by the nonsaturable lipid-mediated pathway and should change E_a for water transport towards that for lipid-mediated transfer (~15 kcal/mol; ref. 11). Changes in surface area due to increasing gradient size should not affect E_a since the pathway across the single barrier remains unchanged. The effect of increasing gradient size on E_a for a vesicle with structural restriction is not predictable without knowledge of the physical mechanism by which restriction takes place. Stopped-flow measurement of water efflux was carried out using both 250 and 500 mM inwardly directed sucrose gradients at 5° intervals between 10 and 50°C. The Arrhenius plots for these data are shown in Fig. 5. The lines drawn through these points are the best fit of a double-connected line as determined by a four-parameter, least-squares fitting procedure. The values for the activation energies and the points of slope discontinuity are given in Fig. 5. Below 27°C the activation energies for 250 and 500 mM gradients were not significantly different and were both approximately 10 kcal/mol. Above 27°C, the activation energy for a 500-mM gradient was significantly greater than that calculated for a 250-mM gradient. The increase

in E_a from 5.4 to 7.3 kcal/mol supports the transport saturation mechanism and does not exclude the structural restriction mechanism.

Flow Dependence of P_f

The final approach used to distinguish between mechanisms was the measurement of P_f under conditions where transmembrane volume flow was varied without altering the initial and final vesicle volumes. P_f measured in the presence of a USL, transport saturation and dynamic structural restrictions would be flow dependent whereas the surface area mechanism is not. The response of a vesicle with a static structural restriction mechanism is not predictable. Three groups of MVV were incubated overnight, in 100, 200 or 300 mM sucrose, 10 mM HEPES-Tris, pH 7.0 (~0.3 mg/ml) and then exposed to inwardly directed sucrose gradients which resulted in a 40% decrease in vesicle volume for each group. Although the absolute vesicle volume change was the same for each group, gradient size ranged from 65 to 200 mM and thus transmembrane volume flow varied > threefold. P_f was $(2.7 \pm 0.3) \times 10^{-3}$ (65-mM gradient), $(2.6 \pm 0.2) \times 10^{-3}$ (130 mM) and $(2.9 \pm 0.5) \times 10^{-3}$ (200 mM) at 23°C. These results suggest that the mechanism operating to decrease P_f at increasing gradient size is not a flow-dependent mechanism.

Water Transport Inhibition Studies

Because the activation energy for water transport above 27°C was similar to that observed for carrier-mediated water transport in the erythrocyte [11], attempts were made to inhibit water transport using sulfhydryl-specific reagents. *p*-Chloro-mercuribenzenesulfonate (5 mM), mercuric chloride (0.5 mM) and iodoacetamide (5 mM) were incubated with MVV for 20 min at room temperature. The time constants for water efflux, determined using a 500-mM sucrose gradient, were 0.098 ± 0.012 sec (*p*CMBS), 0.109 ± 0.015 sec ($HgCl_2$) and 0.099 ± 0.003 sec (iodoacetamide), not significantly different from the control value of 0.093 ± 0.005 sec (n = 8; 23°C). In additional experiments performed at 37°C, MVV containing 100 mM sucrose, 10 mM HEPES-Tris, pH 7.0, were subjected to a 200-mM sucrose gradient after incubation with *p*CMBS (5 mM) for 60 min. The exponential time constants determined were 0.28 ± 0.02 sec (control) and 0.18 ± 0.01 sec (*p*CMBS). Ten mM mercaptoethanol had no effect on the time constants. The apparent acceleration in water efflux due to *p*CMBS was matched by an equivalent fractional acceleration in urea influx (*data not shown*) indicating that *p*CMBS had a nonspecific effect on membrane transport.

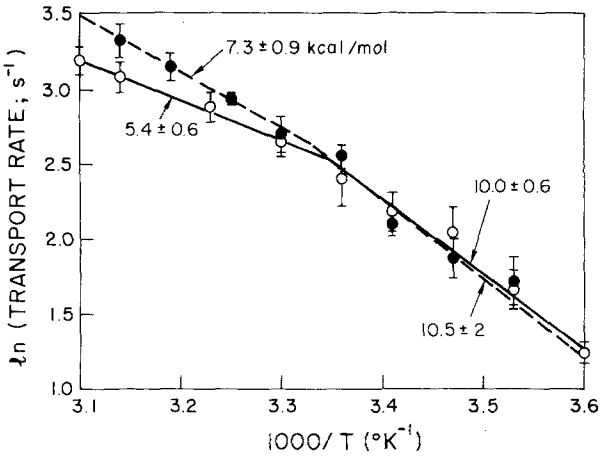

Fig. 5. Temperature dependence of water transport. MVV diluted in buffer A were mixed in a 1:1 ratio with 0.5 M (open circles) or 1.0 M (closed circles) sucrose in buffer A. Results are mean ± SD of five and two preparations, respectively. The activation energies given in the Figure are in units of kcal/mol. The breakpoints for the two curves were 25 ± 3°C and 28 ± 6°C for the 0.5 and 1.0 M curves respectively

Discussion

Two difficulties encountered in determining the permeability coefficients for microvillous vesicles are vesicle size heterogeneity and contamination with nonbrush-border membranes. In order to minimize these problems, an isolation procedure was devised which used the techniques of $MgCl_2$ precipitation and sucrose density gradient centrifugation to remove nonbrush-border membranes and to isolate a single membrane population (MVV-C2) as defined by vesicle density. Comparison of the purification achieved here with literature values is difficult because many reports give only the enrichment of a microvillous membrane marker and omit data on the presence or enrichment of other membranes. The enrichment of alkaline phosphatase shown here is comparable to the higher levels of enrichment in several reports [2, 4, 33]. Like Booth et al. [4] we also observed an coenrichment in aminopeptidase M, but were unable to find any gamma glutamyl transpeptidase activity as reported by Truman et al. [33] in either homogenates or vesicles although it was present in LLC-PK1 cell membranes tested simultaneously. The enrichment of aminopeptidase M was low compared to alkaline phosphatase possibly because of the presence of proteins other than aminopeptidase M in the homogenates which hydrolyse the substrate (L-alanine-naphthylamide) for

the aminopeptidase M assay. The contamination by intracellular membranes such as mitochondria, endoplasmic reticulum and lysosomes was low as evidenced by the de-enrichment of succinate dehydrogenase, NADPH cytochrome *c* reductase and acid phosphatase in MVV relative to homogenate. The major possible plasma membrane contaminant is the syncytiotrophoblast basolateral membrane. Assay of ouabain-sensitive Na^+, K^+-ATPase showed that the basolateral membrane was depleted four-fold relative to homogenate, reducing contamination to a greater extent than that achieved either by Booth et al. [4] or by Whitsett and Wallick [37], reports in which Na^+, K^+-ATPase activity was assayed.

The separation of the crude microvillous preparation into two fractions, C1 and C2, is very similar to that described by Truman et al. [33]. The densities determined by linear sucrose gradient centrifugation and the higher alkaline phosphatase activity in the C2 fraction suggested that our fractions were the same. Truman et al. suggested that the two fractions differed in their internal structure, the C2 fraction showing a decreased content of membrane-associated (possibly cytoskeletal) proteins. SDS/polyacrylamide electrophoresis carried out on the two fractions supported this possibility. We found major reductions in the 42,000, 64,000, 93,000 and 104,000 dalton bands in the C2 fraction, proteins which have been suggested to be actin, villin and alpha-actinin [5]. The increased band at 71,000 in C2 may represent either the increased alkaline phosphatase in this fraction apparent from enzyme assays or the structural protein fimbrin also shown to be present in placental microvilli [5].

Because the C1 and C2 fractions were not interconvertible, the sucrose density gradient separates two subpopulations of MVV. The C2 fraction was chosen for experimental purposes because it demonstrated higher alkaline phosphatase enrichment and reduced contamination relative to the C1 fraction. The homogeneity evidenced by sucrose density-gradient banding suggested that this was a single population of intact vesicles which would be more likely to show defined, reproducible values for osmotic permeability parameters than the C1 fraction. The exponential time constant for water efflux for eight separate C2 preparations, for example, was 0.094 ± 0.004 sec (mean ± SD; 500 mM sucrose gradient at 23°C).

The observation of decreased P_f with increasing gradient size has not been reported previously. P_f is independent of gradient size in human red cells [32], platelets [25] and renal proximal tubule cells [26]. The evidence from a series of experiments summarized in Table 3 and Figs. 3 and 4 suggests that a structural limitation causes the decrease in P_f at higher osmotic gradients. The viscosity experiments ruled out USL's as a cause of the P_f alterations since no change was observed despite the presence of up to 6% dextran. Experiments involving preshrinking of MVV showed that absolute vesicle size was an important influence on P_f since a 50% decrease in vesicle volume produced by preshrinking caused a 35% decrease in P_f. This effect would not occur if USL's or saturation of a water transport mechanism caused the alteration in P_f. The finding that P_f was not flow dependent provided further support for a structural restriction mechanism.

The model used for structural limitation was that of a second, serial barrier to water movement which becomes increasingly important in relation to the primary (membrane) barrier as the vesicle volume decreases. Although our data supports the existence of a structural barrier, it is not possible to define the precise physical characteristics of the structural limitation. The placental brush border has a complex cytoskeletal structure which has only been partially elucidated [5]. It is possible that the structural barrier results from restriction to vesicle volume change imposed by the vesicle cytoskeletal components. Because the nature of this restriction is unknown, it is difficult to predict the effect of temperature on the second barrier (Fig. 5). The observed increase in E_a above 32°C is not consistent, however, with a P_f alteration mechanism involving surface area changes.

Lack of information on the exact nature of the second barrier prevents us from accurately predicting the effects of gramicidin on P_f (Fig. 4). Nevertheless, the prediction based on a simple structural limitation model is the one which best fits the experimental data. The predictions of the structural limitation model also fit the measured dependence of P_f on gradient size (Fig. 3). The curve corresponding to the predictions of the structural limitation model in Fig. 3 has been shown as a constant P_f of 0.003 cm/sec below a 65-mM gradient and decreasing above 65 mM according to the predictions of Eq. (6). This is based on the assumption that structural limitation is unlikely to be symmetric and that at some lower gradient size it will cease to restrict vesicle size change and hence P_f. The point at which the structural limitation curve becomes constant was arbitrarily chosen to fit the data in the light of the other evidence suggesting that this is the mechanism by which P_f is affected. The more than four-fold changes observed in P_f with variation in gradient size suggest that measurement of P_f in membrane vesicle systems should be carried out over a range of gradient sizes so as to detect the

presence of structural barriers and that the true membrane P_f should be based on an extrapolation of data to zero osmotic gradient.

In comparison with other bilayer membranes, the placental microvillous membrane has a low osmotic water permeability.[2] The P_f for MVV at 37°C is 4.8×10^{-3} cm/sec compared to 7.7×10^{-3} cm/sec for human platelets [25], 11×10^{3} cm/sec for rabbit renal brush-border vesicles [35], 18.3×10^{-3} cm/sec for rat brain synaptosomes [36] and 27×10^{-3} cm/sec for erythrocytes [27]. The P_f for MVV is higher than that normally found for synthetic bilayer membranes which have osmotic permeability coefficients in the range 0.6 to 1.0×10^{-3} cm/sec [11]. Addition of gramicidin increased the permeability of MVV but the fractional increase in P_f was less than that observed by Worman and Field in the rat intestinal brush border [39]. They observed an increase in P_f from 1.2×10^{-3} to 4.8×10^{-3} cm/sec after gramicidin treatment (175 mM mannitol gradient, 23°C). The absolute change in P_f for MVV using a 250-mOsm sucrose gradient was similar in magnitude, from 3.0×10^{-3} to 5.5×10^{-3} at 23° after treatment with gramicidin. Gramicidin appeared to introduce an incremental P_f of ~0.003 cm/sec.

The Arrhenius plots for water transport (Fig. 5) are notable in two ways. The first is the low activation energies (E_a) for water transport measured using a 250-mM hyperosmotic sucrose gradient (E_a = 4.7 ± 1.1 kcal/mol, $T > 27$°C; E_a = 7.3 ± 1.7 kcal/mol, $T < 27$°C). The second is the discontinuity observed in the activation energy for water transport at 26 ± 3°C and 28 ± 6°C for curves measured using 250 and 500 mM sucrose gradients. Activation energies in the range of 4 to 5 kcal/mol have been observed previously in mammalian erythrocytes [12] and in rabbit cortical collecting tubules in the presence of vasopressin [14]. These values are the same as that for the self-diffusion of water and are generally associated with mediated processes for water transport such as specific carriers or transport via aqueous pores or channels. The low E_a for water transport above 27°C in MVV may be associated with passage of water through an aqueous channel. In the erythrocyte, water transport is 90% inhibited by *p*CMBS and a number of other organic mercurial sulfhydryl reagents [24]. Attempts to inhibit MVV water transport with $HgCl_2$, *p*CMBS and iodoacetamide proved unsuccessful. It is possible, however, that placental brush border contains a protein-mediated water channel which is unlike that of the erythrocyte and which is insensitive to sulfhydryl modification reagents. Another possibility which might account for the low E_a above 27°C is nonspecific water transport, taking place at the interface between protein and lipid, as suggested by Carruthers and Melchior [8]. The higher E_a observed below 27°C is more consistent with a lipid-mediated transport pathway for water [3], either by a solubility-diffusion mechanism or via transient pores [15]. Seeds et al. [30] reported values less than 5 kcal/mol for the activation energy of diffusional water transport across human amnion and chorion, and concluded that transport took place primarily via extracellular water-filled channels. The data reported here suggest that this interpretation is not necessarily the correct one.

The discontinuity in the Arrhenius plot of water transport has two possible interpretations. The presence of serial permeability barriers is consistent with decreased E_a above the temperature of the discontinuity, where permeabilty is most restricted by the barrier with lower E_a. As the osmotic gradient size increases (0.5 to 1 M), E_a above the transition temperature increases from 5.4 to 7.3 kcal/mol, consistent with a change in the physical characteristics of the nonmembrane permeation barrier.

Alternatively, the biphasic Arrhenius plot is consistent with the presence of a thermotropic membrane lipid phase transition which may alter the properties of water transport through lipid or at the protein-lipid interface. This possibility is supported by a similar discontinuity in the Arrhenius plot of MVV urea transport at 27 ± 2°C [18], and in the Arrhenius plots of Na^+/H^+ transport (28 ± 2°C) and the activities of several brush-border enzymes (alkaline phosphatase, 28 ± 1°C; aminopeptidase M, 31 ± 3°C, ref. 17). There is strong additional evidence obtained from fluorescence lifetime heterogeneity analyses of *cis*- and *trans*-parinaric acids, which show transition in lipid phase from solid to fluid centered at 27°C. Differential polarization measurements of the limiting anisotropy of diphenylhexatriene (DPH) support the presence of a thermotrophic phase transition in the temperature range 24 to 29°C in these vesicles [17]. Thus alterations in lipid-packing dynamics may modulate the transmembrane passage of water. Further definition of the nature of the placental water pathway will require chemical modification of the membrane phospholipid and protein structure, and target size determination by radiation inactivation.

[2] Wilbur et al. [38] have estimated a whole organ filtration coefficient of 2.0×10^{-6} liter/sec · mm Hg. Assuming that $P_f = P_d$ (diffusional water permeability coefficient), and using a value for total trophoblastic surface area at term of 67 m² [31], we calculated a value for P_f from this filtration coefficient of 4.9×10^{-3} cm/sec, which is similar to the value we determined experimentally of 4.8×10^{-3} cm/sec. Because of the uncertainties in these estimates, it is difficult to determine whether the primary route for water transport is transcellular.

We thank the staff of the labor and delivery ward at University of California, San Francisco Medical Center for help in obtaining placental tissue. This work was supported by NIH grant AM35124, grants from the U.C.S.F. Academic Senate and MSC Clough Fund and from the National Cystic Fibrosis Foundation. Dr. Illsley was supported by NIH training grant AM07219.

References

1. Barry, P.H., Diamond, J.M. 1984. Effect of unstirred layers on membrane phenomena. *Physiol. Rev.* **64:**763–872
2. Bissonnette, J.M., Black, J.A., Wickham, W.K., Acott, K.M. 1981. Glucose uptake into plasma membrane vesicles from the maternal surface of human placenta. *J. Membrane Biol.* **58:**75–80
3. Bittman, R., Blau, L. 1972. The phospholipid-cholesterol interaction kinetics of water permeability in liposomes. *Biochemistry* **11:**4831–4839
4. Booth, A.G., Olaniyan, R.O., Vanderpuye, O.A. 1980. An improved method for the preparation of human placental syncytiotrophoblast microvilli. *Placenta* **1:**327–336
5. Booth, A.G., Vanderpuye, O.A. 1983. Structure of human placental microvilli. *CIBA Foundation Symposium* **95:**180–194
6. Bowers, G.N., McComb, R.B. 1966. A continuous spectrophotometric method for measuring the serum activity of alkaline phosphatase. *Clin. Chem.* **12:**70–89
7. Boyd, C.A.R., Lund, E.K. 1981. L-proline transport by brush border membrane vesicles prepared from human placenta. *J. Physiol. (London)* **315:**9–19
8. Carruthers, A., Melchior, D.L. 1983. Studies of the relationship between bilayer water permeability and bilayer physical state. *Biochemistry* **22:**5795–5807
9. Cole, D.E.C. 1984. Sulfate transport in brush border membrane vesicles prepared from human placental syncytiotrophoblast. *Biochem. Biophys. Res. Commun.* **123:**223–229
10. Elbers, P.F., Ververgaert, P.H.J.T., Demel, R. 1965. Tricomplex fixation of phospholipids. *J. Cell Biol.* **24:**23–30
11. Fettiplace, R., Haydon, D.A. 1980. Water permeability of lipid membranes. *Physiol. Rev.* **60:**510–550
12. Forster, R.E. 1971. The transport of water in erythrocytes. *Curr. Top. Membr. Transp.* **2:**41–98
13. George, S.G., Kenny, A.J. 1973. Studies on the enzymology of purified preparations of brush border from rabbit kidney. *Biochem. J.* **134:**43–57
14. Hebert, S.C., Andreoli, T.E. 1972. Interactions of temperature and ADH on transport processes in cortical collecting tubules. *Am. J. Physiol.* **238:**F470–F480
15. Huang, C., Thompson, T.E. 1966. Properties of lipid bilayer membranes separating two aqueous phases: Water permeability. *J. Mol. Biol.* **15:**539–554
16. Hutchison, D.L., Gray, M.J., Plentl, A.A., Alvarez, H., Caldeyro-Barcia, R., Kaplan, B., Lind, J. 1959. Role of the fetus in the water exchange of the amniotic fluid of normal and hydamniotic patients. *J. Clin. Invest.* **38:**971–980
17. Illsley, N.P., Lin, H.Y., Verkman, A.S. 1986. Lipid domain structure correlated with membrane protein function in placental microvillus vesicles. *Biochemistry (in press)*
18. Illsley, N.P., Verkman, A.S. 1986. Water and urea transport across the microvillous membrane of the human placenta. *Placenta (Abstr.)* **7:**481
19. Ives, H.E., Yee, V.J., Warnock, D.G. 1983. Asymmetric distribution of the Na^+/H^+ antiporter in the renal proximal tubule epithelial cell. *J. Biol. Chem.* **258:**13513–13516
20. Johnson, L.W., Smith, C.H. 1980. Monosaccharide transport across microvillous membrane of human placenta. *Am. J. Physiol.* **238:**C160–C168
21. Karnovsky, M.J. 1965. A formaldehyde-glutaraldehyde fixative of high osmolality for use in electron microscopy. *J. Cell. Biol.* **27:**137A–138A
22. Laemmli, U.K. 1970. Cleavage of structural proteins during the assembly of the head of bacteriophage T4. *Nature (London)* **227:**680–685
23. Lowry, O.H., Rosebrough, N.J., Farr, A.L., Randall, R.J. 1951. Protein measurement with the Folin phenol reagent. *J. Biol. Chem.* **193:**265–275
24. Macey, R.I. 1984. Transport of water and urea in red blood cells. *Am. J. Physiol.* **246:**C195–C203
25. Meyer, M.M., Verkman, A.S. 1986. Human platelet osmotic water and non-electrolyte transport. *Am. J. Physiol.* **251:***C*549–*C*557
26. Meyer, M.M., Verkman, A.S. 1987. Water channels are present in renal proximal tubule cell membranes. *Biophys. J. (abstr.) (in press)*
27. Rabon, E., Takeguchi, N., Sachs, G. 1980. Water and salt permeability of gastric vesicles. *J. Membrane Biol.* **53:**109–117
28. Reeves, J.P., Dowben, R.M. 1970. Water permeability of phopholipid vesicles. *J. Membrane Biol.* **3:**123–141
29. Schoner, W., Ilberg, C. von, Kramer, R., Seubert, W. 1967. On the mechanism of Na^+- and K^+-stimulated hydrolysis of adenosine triphosphate. 1. Purification and properties of a Na^+- and K^+-activated ATPase from ox brain. *Eur. J. Biochem.* **1:**334–343
30. Seeds, A.E., Schruefer, J.J., Reinhardt, J.A., Garlid, K.D. 1973. Diffusion mechanisms across human placental tissue. *Gynecol. Invest.* **4:**31–37
31. Teasdale, F., Jean-Jacques, G. 1985. Morphormetric evaluation of the microvillous surface enlargement factor in the human placenta from mid-gestation to term. *Placenta* **6:**375–381
32. Terwilliger, T.C., Solomon, A.K. 1981. Osmotic water permeability of human red cells. *J. Gen. Physiol.* **77:**549–570
33. Truman, P., Wakefield, J.St.J., Ford, H.C. 1981. Microvilli of the human term placenta. *Biochem. J.* **196:**121–132
34. Veeger, C., DerVartanian, D.V., Zeylemaker, W.P. 1969. Succinate dehydrogenase. *Methods Enzymol.* **13:**81–90
35. Verkman, A.S., Dix, J.A., Seifter, J.L. 1985. Water and urea transport in renal microvillus membrane vesicles. *Am. J. Physiol.* **248:**F650–F655
36. Verkman, A.S., Fraser, C.L. 1986. Water and nonelectrolyte permeability in brain synaptosomes isolated from normal and uremic rats. *Am. J. Physiol.* **250:**R306–R312
37. Whitsett, J.A., Wallick, E.T. 1980. [H^3]Ouabain binding and Na^+/K^+ ATPase activity in human placenta. *Am. J. Physiol.* **238:**E38–E45
38. Wilbur, W.J., Power, G.G., Longo, L.L. 1978. Water exchange in the placenta: A mathematical model. *Am. J. Physiol.* **235:**R181–R199
39. Worman, H.J., Field, M. 1985. Osmotic water permeability of small intestinal brush-border membranes. *J. Membrane Biol.* **87:**233–239

Received 9 June 1986; revised 19 August 1986